FULL-WAVE SPECTRAL-DOMAIN ANALYSIS OF COMPENSATION OF MICROSTRIP DISCONTINUITIES USING TRIANGULAR SUBDOMAIN FUNCTIONS†

Tzyy-Sheng Horng, William E. McKinzie and Nicolaos G. Alexopoulos

Electrical Engineering Department

University of California, Los Angeles

Los Angeles, Ca 90024

† This research was supported by National Science Foundation Research Grant ECS 8802617

Abstract

This paper presents a full-wave spectral-domain analysis to investigate compensation of a variety of microstrip discontinuities including bends and T junctions. To properly model the discontinuities with miters as well as 90° corners, vector-valued triangular subdomain functions are used as both expansion and testing functions in the moment method procedure. Special consideration is given to the numerical treatment of the reaction integral between two triangular subdomains such that rather complicated geometrical configurations can be handled very efficiently. Comparison of some numerical results with available experimental data shows excellent agreement. The losses due to radiation and surface waves in some discontinuities will also be discussed in the presentation.

I. INTRODUCTION

In the design of microwave and millimeter wave circuits, compensation of microstrip discontinuities is widely used to reduce the effects of discontinuity reactances [1]. For low frequency applications, quasi-static analysis has been successfully applied to compensation of some discontinuities such as steps, right-angle bends and T junctions [2]-[3]. At higher frequencies, a dynamic model based on a full-wave analysis is required to take into account more physical effects such as radiation and surface-wave losses. The most rigorous full-wave method for the characterization of open microstrip discontinuities is governed by the well-known electric field integral equation (EFIE), which can be formulated in both the space domain and spectral domain. In the space domain, the dyadic kernel in the EFIE is the Green's function for the electric field which can be obtained from a Sommerfeld-type integral. Since the kernel is highly singular, the evaluation of the reaction integrals in the moment method procedure is difficult when the observation point is within the integration range. The spectral-domain analysis performs an integral transformation, usually Fourier or Hankel transforms, to transform a partial differential equation into an ordinary differential equation. After satisfying the boundary conditions at the interfaces of multi-layer stratified dielectric medium, this approach can lead to a closed-form expression for the so called spectral-domain dyadic Green's function. The space-domain electromagnetic fields can be further expressed by taking the inverse Fourier transform of the vector product of this spectral-domain dyadic Green's function and Fourier transform of the microstrip currents. Such an EFIE formulation in the spectral-domain has several advantages over the space-domain method including a better behaved integrand in the reaction integral and easier calculation for both radiation and surface-wave losses. Hence, one can compute the impedance matrix in the moment of moments very accurately such that the circuit parameters in a microstrip junction can be rigorously determined.

A review of past work using full-wave spectral-domain analysis for open microstrip discontinuities reveals that the technique developed up to now is limited to a multi-port junction whose shape can be divided into a number of rectangles. The most commonly used expansion functions, pulse and piecewise sinusoidal functions, are appropriate only for modeling a discontinuity with 90° corners. To model the discontinuities with miters at any angle, vector-valued triangular subdomain functions are adopted in this analysis as both expansion and testing functions in the moment method procedure. These triangular subdomain functions were apparently first employed by Rao, Wilton and Glisson [4]. They are suitable for modeling electric currents on arbitrary PEC surfaces. However, the present application will restrict the surface patches to lie in the plane of discontinuities. Since a spectral-domain approach is employed in the characterization of microstrip discontinuities, the Fourier transform of the triangular subdomain function has to be derived. This results in a very complicated mathematical expression. Crucial to the numerical formulation is the efficient computation of the reaction integrals associated with these triangular subdomains to avoid tremendous CPU time. An efficient method to improve CPU time is to employ a space-domain technique for the asymptotic solution of the spectral-domain reaction integral [5].

II. SPECTRAL-DOMAIN MATRIX FORMULATION

A. Electric Field Integral Equation

Consider a microstrip structure where the current distribution over the microstrip discontinuities is treated in terms of a number of infinitesimal dipoles continuously distributed on the interface between the dielectric and the air. From linear superposition, the tangential electric field on

CH3141-9/92/0000-107$01.00 © 1992 IEEE

the interface can be expressed by a two-dimensional spatial convolution of the dyadic Green's function with the current distribution. Each component of this two-dimensional spatial convolution corresponds to multiplication of the two-dimensional Fourier transforms in the spectral domain. Therefore, the space-domain tangential electric field can be expressed again as an inverse Fourier transform of the vector product of spectral-domain dyadic Green's function and the Fourier transform of the microstrip currents. With the boundary condition that such field is zero on the perfectly conducting microstrips, an electric field integral equation can be set up:

$$\vec{E}_t(x,y) = \frac{1}{4\pi^2}\int_{-\infty}^{\infty}\int_{-\infty}^{\infty}\overline{\overline{G}}(k_x,k_y)\cdot\vec{J}(k_x,k_y) \\ e^{-jk_x x}e^{-jk_y y}dk_x dk_y = 0, \text{ for } x,y \text{ on microstrips} \quad (1)$$

where $\overline{\overline{G}}$ and $\vec{J}$ are the spectral-domain dyadic Green's function and the current distribution respectively. The spectral-domain dyadic Green's function which can be derived in closed form takes into account all the physical phenomena including radiation and surface waves.

B. Triangular Subdomain Functions

The triangular subdomain functions as shown in Fig. 1 are vector-valued functions defined as

$$\vec{f}_p(x,y) = \begin{cases} \frac{l_p}{2A_p^+}(x-x_3, y-y_3), & x,y \text{ in } T_p^+ \\ \frac{l_p}{2A_p^-}(x_4-x, y_4-y), & x,y \text{ in } T_p^- \\ 0, & \text{otherwise} \end{cases} \quad (2)$$

where T_p^+ and T_p^- denote the faces of two triangles with areas A_p^+ and A_p^- respectively. Fig. 1 also shows a microstrip discontinuity of arbitrary shape on a substrate with permittivity ϵ and substrate thickness h. This discontinuity is inscribed with non-overlapping triangles defined in terms of an appropriate set of vertices, faces, interior edges and boundary edges. The p^{th} expansion function ($\vec{f}_p$) is uniquely associated with a pair of adjacent triangles with an jointed edge (interior edge) whose length is l_p. The current on microstrip can be expanded as

$$\vec{J}(x,y) \simeq \sum_{p=1}^{N} I_p \vec{f}_p(x,y) \quad (3)$$

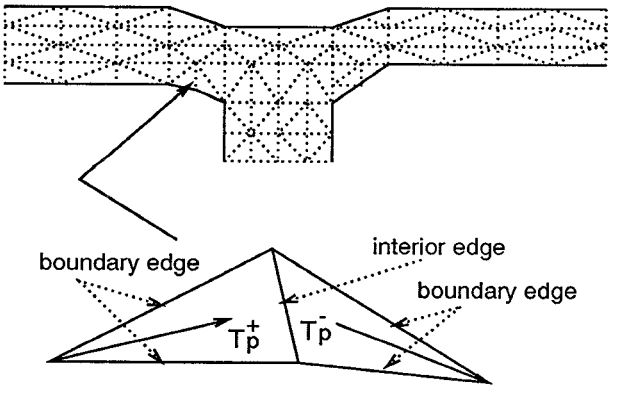

Fig. 1. Triangular subdomain function

where N is the total number of the interior edges and I_p are unknown coefficients to be obtained through the method of moments. Each basis function has two salient properties which can make it uniquely suited to approximate electric surface currents on microstrip discontinuities of arbitrary shape [4] :

- The current has no component normal to the boundary edge.
- The component of current normal to the p^{th} interior edge is constant and continuous across the edge.

The triangular subdomain function basically consists of a pair of linearly varying functions with triangular support whose Fourier transform can be found in [6]. After arrangement, the Fourier transform of $\vec{f}_p(x,y)$ can be easily derived. The Fourier transform is defined as

$$\tilde{\vec{f}}_p(k_x,k_y) \equiv \int_{T_p^+ + T_p^-}\int_{T_p^+ + T_p^-}\vec{f}_p(x,y)e^{jk_x x}e^{jk_y y}dxdy. \quad (4)$$

C. Galerkin's Procedure

After substituting the expanded current expression (3) and the Fourier transforms of expansion functions (4) into (1), the method of moments can be applied to convert this integral equation into a matrix equation. The testing functions in the moment method procedure are also chosen to be triangular subdomain functions. As a result, the matrix equation for a microstrip discontinuity is generally formulated as

$$[Z]_{N\times N}[I]_N = [V]_N. \quad (5)$$

Each matrix element in $[Z]$ represents the reaction between two basis functions. The computation of each element requires a double infinite integration in the spectral domain:

$$Z_{mn} = \frac{1}{4\pi^2}\int_{-\infty}^{\infty}\int_{-\infty}^{\infty}\left[\overline{\overline{G}}(k_x,k_y)\cdot\tilde{\vec{f}}_n(k_x,k_y)\right]\cdot\tilde{\vec{f}}_m^{*}(k_x,k_y)dk_x dk_y \quad (6)$$

where the superscript $*$ represents the complex conjugate of the function. In (5), the right-hand side matrix represents an excitation mechanism for the microstrip junction. In this analysis, an ideal delta-gap voltage source is used to excite the junction.

III. NUMERICAL EVALUATION OF MATRIX ELEMENTS

After transforming into polar coordinates, the double infinite integration in (6) is carried out numerically. We reduce the integration to a finite integral (0 to 2π) with respect to an angular variable $\theta = \tan^{-1}\frac{k_y}{k_x}$ and an infinite integral (0 to ∞) with respect to a radial variable $\lambda = \sqrt{k_x^2+k_y^2}$. For the finite integral, since the integrand is smoothly behaved over the angular domain, a 16 to 48 Gaussian quadrature formula is used depending on the distance between the expansion and testing functions. For the infinite integral, the integrand containing the Fourier transforms of triangular subdomain expansion and testing functions is mathematically complex and converges slowly. Solutions to impedance matrix elements take approximately 4 times the CPU time when compared to the integrand using pulse or piecewise sinusoidal functions in modeling the discontinuities with 90°

corners. An efficient method to perform the integration is to apply an asymptotic extraction technique. This technique breaks the double infinite integral into two integrals. One is the asymptotic integral (denoted by Z^a_{mn}) where the leading term of asymptotic expansion of $\overline{\overline{G}}$ as $\lambda \to \infty$ is used in the integrand. The other is the difference integral (denoted by Z^d_{mn}) where subtraction of this leading term from $\overline{\overline{G}}$ is used in the integrand. After a slight arrangement, it is found that the leading term of asymptotic expansion of $\overline{\overline{G}}$ is asymptotically equivalent to the dyadic Green's function in a homogeneous medium (denoted by $\overline{\overline{G}}_h$) with the dielectric constant equal to the average of the dielectric constants immediately above and below the source points. As a result, both integrals can be mathematically expressed as follows.

$$Z_{mn} = Z^a_{mn} + Z^d_{mn} \tag{7}$$

where

$$Z^a_{mn} = \int_0^\infty \int_0^{2\pi} \left[\overline{\overline{G}}_h(\lambda,\theta) \cdot \vec{f}_n(\lambda,\theta)\right] \cdot \vec{f}^*_m(\lambda,\theta)\lambda d\theta d\lambda \tag{8}$$

and

$$Z^d_{mn} = \int_0^\infty \int_0^{2\pi} \left[(\overline{\overline{G}}(\lambda,\theta) - \overline{\overline{G}}_h(\lambda,\theta)) \cdot \vec{f}_n(\lambda,\theta)\right] \cdot \vec{f}^*_m(\lambda,\theta)\lambda d\theta d\lambda. \tag{9}$$

With this technique, fast convergence for the difference integral can be obtained. It is observed that the convergence of the integral in (9) is improved by the order of λ^2 when compared to the integral in (6).

In this analysis, both asymptotic and difference integrals are calculated very efficiently. The asymptotic integral in (8) represents the mutual impedance between the expansion function $\vec{f}_n$ and the testing function $\vec{f}_m$ in an infinite homogeneous medium. We evaluated this integral in the space domain by employing a numerical method similar to that used by Rao et al [4]. For the difference integral, the infinite integration range in (9) with respect to λ can be truncated within $(0, A)$ due to the fast convergence. A must be chosen large enough to satisfy $\overline{\overline{G}} \simeq \overline{\overline{G}}_h$ as $\lambda > A$, which can result from

$$\sqrt{A^2 - k_0^2\epsilon} \simeq A \tag{10}$$

and

$$\tanh Ah \simeq \coth Ah \simeq 1. \tag{11}$$

From (10) and (11), it can be concluded that the determination of A depends on dielectric constant and electric thickness of the substrate. For larger dielectric constant or electrically thicker substrates, A can be chosen smaller to cause less numerical expense in evaluation of the difference integral. Moreover, the integrand in (9) contains all the singularities, namely the surface wave poles, over the λ domain. One way of performing the integration from 0 to A is to deform the contour off the real axis and apply the Cauchy Riemann theorem such that the integrand is well behaved [7]. This method is particularly useful in a multi-layered structure because knowledge of individual pole locations is not required. The evaluation of the difference integral can be considered as the key contribution from the multi-layered structure to each impedance matrix element. It includes the surface-wave resistance and part of the radiation resistance in each element.

Although the spectral-domain difference integral has been reduced to a double finite one with well-behaved integrand, we may further reduce CPU time by employing some special numerical schemes developed in the spectral domain. These schemes will be introduced in the presentation.

IV. NUMERICAL RESULTS AND DISCUSSION

A. An Open-End Discontinuity

To demonstrate the numerical accuracy of this analysis, the phase term of the reflection coefficient calculated from an open end has been compared with the measurements in [8] and theoretical results in [10]. Fig. 2 shows the comparisons and it is seen that the difference among these three curves is less than 1° over the frequency range of the measurement.

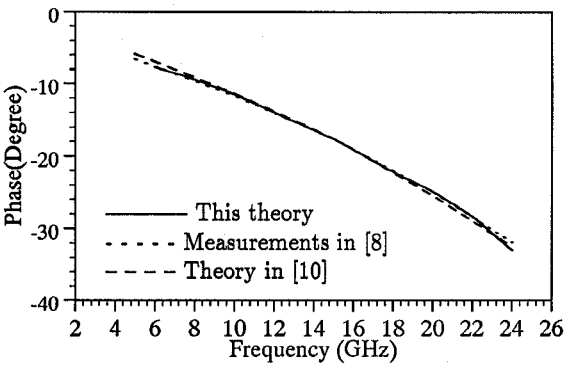

Fig. 2. Phase of S parameters of an open-end. (ϵ=9.9,w=24mil, h=25mil)

B. Bend and T-Junction Discontinuities

The improvements provided by geometrical modification to the outer portion of the right-angle bend with a 45° miter (shown in Fig. 3) are investigated. Fig. 4 shows the normalized susceptance for both right-angle and mitered bend discontinuities as a function of frequency. As expected, the mitered bend has a smaller susceptance than the right-angle bend over a wide frequency range of interest. Comparison of numerical results with measurements in [9] shows excellent agreement.

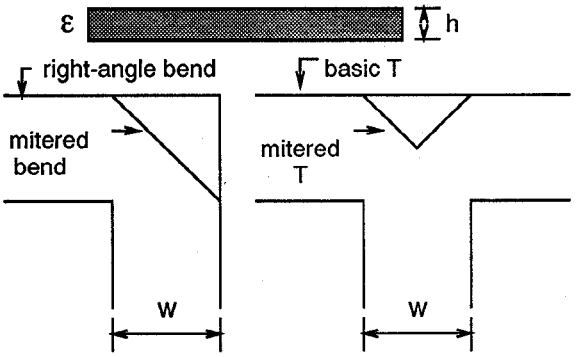

Fig. 3. Compensation of microstrip discontinuities.

For compensation of discontinuity reactances of a basic T junction, the removal of a 45° isosceles triangle is considered. Both discontinuities, basic and mitered T junctions, are shown in Fig. 3. The magnitude of scattering parameters for both discontinuities is shown in Fig. 5, where the comparison with the measured results in [10] for the case of basic T junction shows excellent agreement. It is observed that the improvements of a mitered T junction are pronounced at higher frequencies. Fig. 6 shows the magnitude of electric surface currents which result from a full-wave moment method solution on a mitered T junction at the frequency of 24 GHz.

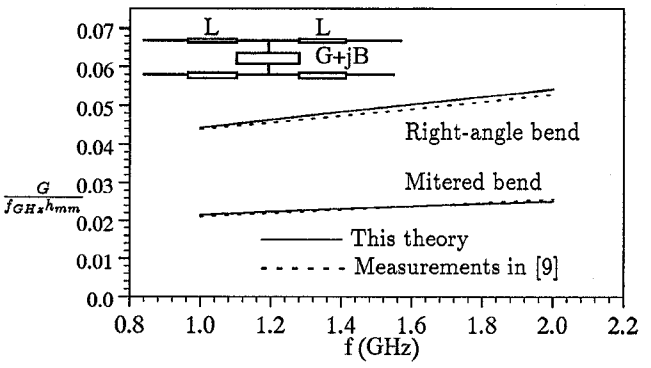

Fig. 4. Normalized susceptance of right-angle and mitered bend discontinuities. (ϵ=10.8,w=4.572mm,h=5.08mm)

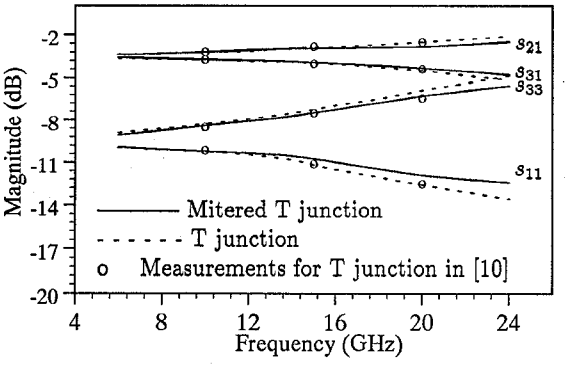

Fig. 5. Magnitude of S parameters of basic and mitered T junctions. (ϵ=9.9, w=24mil, h=25mil)

V. CONCLUSIONS

The full-wave spectral-domain analysis combined with the method of moments using triangular subdomain functions has been found to be a very accurate method to analyze compensation of microstrip discontinuities. Several examples including open-end, right-angle bend, mitered bend, basic T and mitered T junctions were investigated. The numerical results were verified by comparison with available measured data for most of the cases. The comparison showed excellent agreement.

REFERENCES

[1] M. Dydyk, "Master the T-junction and sharpen your MIC designs," Microwaves, vol. 16, no. 5, pp. 184-186, May 1977.

[2] R. Mehran, "Compensation of microstrip bends and Y-junctions with arbitrary angle," IEEE Trans. Microwave Theory Tech., vol. MTT-26, pp. 400-405, June 1978.

[3] R. Chadha and K.C. Gupta,"Compensation of discontinuities in planar transmission lines," IEEE Trans. Microwave Theory Tech., vol. MTT-30, pp.2151-2156, Dec. 1982.

[4] S.M. Rao, D.R. Wilton, and A.W. Glisson, "Electromagnetic scattering by surfaces of arbitrary shape," IEEE Trans. Antennas Propagat., vol. AP-30, pp.409-418, May 1982.

[5] D.M. Pozar, "Improved computational efficiency for the method of moments solution of printed dipoles and patch," Electromagnetics, vol. 3, pp. 299-309, 1983.

[6] B. Houshmand, W.C. Chew and S.W. Lee, "Fourier transform of a linear distribution with triangular support and its applications in electromagnetics," IEEE Trans. Antennas Propagat., vol. AP-39, pp. 252-254, Feb. 1991.

[7] E.H. Newman and D. Forrai, "Scattering from a microstrip patch," IEEE Trans. Antennas Propagat., vol. AP-35, pp. 245-251, March 1987.

[8] G. Gronau and I. Wolff, "A simple broad-band device de-embedding method using an automatic network analyzer with time-domain option," IEEE Trans. Microwave Theory Tech., vol. MTT-37, pp. 479-483, March 1989.

[9] R.J.P. Douville and D.S. James, "Experimental study of symmetric microstrip bends and their compensation," IEEE Trans. Microwave Theory Tech., vol. MTT-26, pp. 175-182, March 1978.

[10] S.C. Wu, H.Y. Yang, N.G. Alexopoulos and I. Wolff, "A rigorous dispersive characterization of microstrip cross and T junctions," IEEE Trans. Microwave Theory Tech., vol. MTT-38, pp. 1837-1990, Dec. 1990.

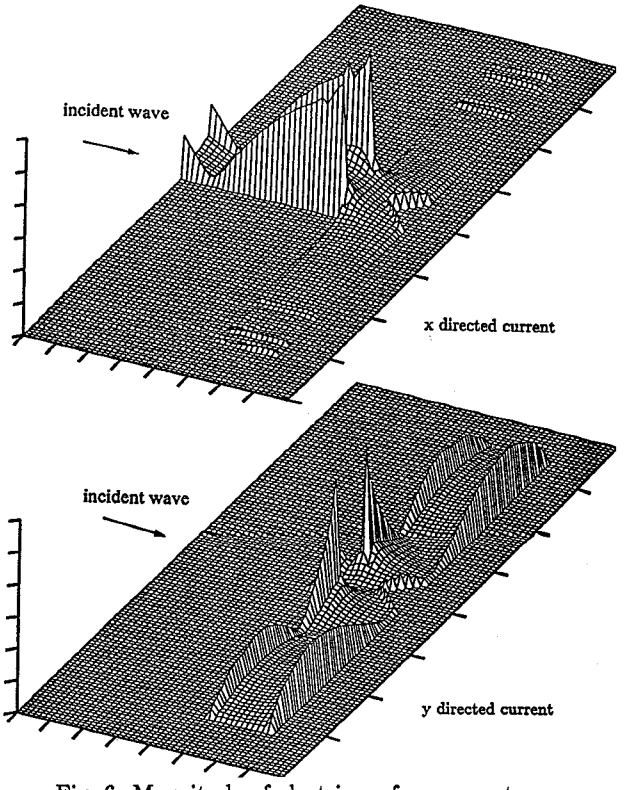

Fig. 6. Magnitude of electric surface currents on a mitered T junction.